Vocational Training Council
VTC Institutional Repository

Staff Publications | Engineering

2021

Improvement of the Autodriver Algorithm for Autonomous Vehicles Using Roll Dynamics

Ching Nok, Catter To
Hong Kong Institute of Vocational Education (Tsing Yi), Vocational Training Council, catter@vtc.edu.hk

Sina Milani
RMIT University

Hormoz Marzbani
RMIT Univeristy, hormoz.marzbani@rmit.edu.au

Reza Jazar
RMIT University, reza.nakahiejazar@rmit.edu.au

Follow this and additional works at: https://repository.vtc.edu.hk/ive-eng-sp

 Part of the Mechanical Engineering Commons

Recommended Citation

To, C.,Milani, S.,Marzbani, H.,& Jazar, R. (2021). Improvement of the Autodriver Algorithm for Autonomous Vehicles Using Roll Dynamics. *The Archives of Automotive Engineering – Archiwum Motoryzacji, 91* (1/2021), 5-23. http://dx.doi.org/https://doi.org/10.14669/AM.VOL91.ART1

This Journal Article is brought to you for free and open access by the Engineering at VTC Institutional Repository. It has been accepted for inclusion in Staff Publications by an authorized administrator of VTC Institutional Repository. For more information, please contact wchu@vtc.edu.hk.

Improvement of Autodriver Algorithm for Autonomous Vehicles Using Roll Dynamics

Abstract

The autodriver algorithm was introduced as a path-following algorithm for autonomous vehicles, which uses road geometry data and planar vehicle dynamics. In this paper, the autodriver algorithm is improved according to practical implications, and a more realistic vehicle model (roll mode) is used, which considers roll degree of freedom in addition to a planar motion. A Ghost-Car path-following approach is introduced to define the desired location of the car at every instance. Key steady-state characteristics of turning vehicles, namely the curvature, yaw rate, and side-slip responses, are discussed and used to construct a feed-forward component of a path-following controller based on the autodriver algorithm. Feedback control loops are designed and applied to minimise transient errors between the road and vehicle positions. Finally, simulations are performed to analyse the path-following performance of the proposed scheme. The results show promising performance of the controller both in terms of error minimisation and passenger comfort.

Keywords— Autonomous Vehicle, Path-Following Control, Road Curvature, Vehicle Roll Dynamics

LIST OF KEY SYMBOLS

$v_{x/y}$	longitudinal/lateral velocity at centre of gravity	S_κ	curvature response
β	side-slip angle at centre of gravity	S_r	yaw rate response
r	yaw velocity	S_β	side-slip response
φ	roll angle	$C_{\alpha f/r}$	front/rear axle's cornering stiffness
p	roll rate (rolling velocity)	ρ	radius of curvature
$I_{x/z}$	roll/yaw moment of inertia	${}^{B}R_{A}$	transformation matrix from A-frame to B-frame
δ	steer angle input	${}^{A}\mathbf{r}$	position vector expressed in a-frame
$a_{1/2}$	distance from front/rear axle		

1) INTRODUCTION

The autonomous vehicle is a fashionable topic and has been a significant focus of research in recent years [1]. The autopilot system is now categorised in different levels of autodriving which can make semi to fully self-drive the vehicle by a set of developed theory. Companies around the world work hard on the software and hardware that aim to control the vehicle in a smarter way. An ultimate smart system is to use the lateral controller for designing dynamic path tracking as a critical component of the control system. This top smart system can guide a vehicle with no human control or can assistant humans to control the vehicle when driving. Many countries use autonomous transportation well. The application of autonomous vehicles using self-drive systems is capable of being applied to cargo, naval steering, military, aircraft and even spacecraft. Autopilot functions can reduce human faults and errors, reducing driving stress. In this article, a full study of the autodriver algorithms on ground vehicles emerge and pursues improvements in the area of vehicle roll dynamics using mathematical theory and make it applicable to a practical model. The study aims to design and implement a control system which makes the autodriver theoretical roll model applicable to a real vehicle.

Implementing a feedback PID control to eliminate the autodriver algorithm errors was expanded in 2018 [10]. A newly developed algorithm is based on a well-defined road expressed mathematically in a global coordinate frame. At any point of the curve, the curvature centre can be calculated and compare, so that allow to follow its curvature centre's loci and turn at the right circle of curvature. The steady-state and transient responses of turning vehicles and the vehicle's resulting path of motion have been investigated. The effect of acceleration can be changed by forwarding velocity. By comparing the vehicle's two responses on the roll model, the result could be used to prove the difference between the steady-state and transient

state response of the centre of rotation of the vehicle in engineering applications. The engineering approximations are well presented and constitute proof of the dynamic vehicle theory using a parameter for steering angle and variable forwarding velocity. More specifically, the dynamic rotation centre of vehicles is determined and compared with steady-state values. The result is essential to design the autodriver algorithm for autonomous vehicles. Moreover, a roll model is more accurate to predict the actual phenomenon of the vehicle.

In the context of autonomous vehicles, the roll angle constituents assume significant and critical importance, and such vehicles are well governed by linear/bicycle equations of motion. Roll movement, before pitch, yaw, and bounce, is the most unpleasant movement for passengers. This objective of this article is the minimisation of roll motion and its fluctuation by applying vehicle roll dynamics.

2) PLANAR-ROLL VEHICLE DYNAMICS

EQUATIONS OF MOTION

The model vehicle in this study (the bicycle-roll model) is based on a rigid rollable vehicle moving in the osculating plane of the road. The equations of motion of the bicycle-roll vehicle model (Figure 1), attached to the vehicle body at its mass centre C, are governed by the following set of nonlinear coupled ordinary differential equations .

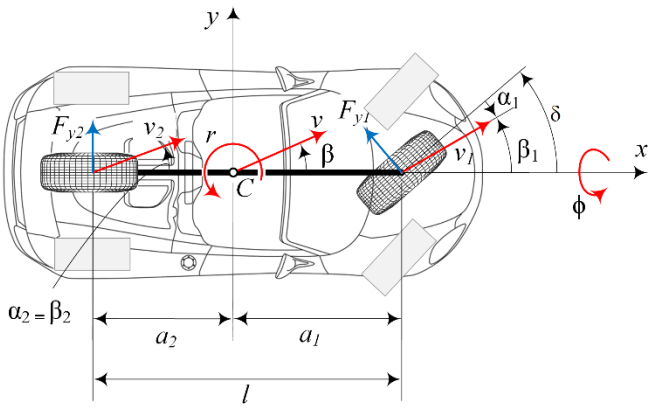

Figure 1: Bicycle-Roll Vehicle Model

$$\dot{v}_x = \frac{F_x}{m} + r v_y \tag{1}$$

$$\dot{v}_y = \left(\frac{C_r}{m} - v_x\right) + \frac{C_p}{m} p + \frac{C_\beta}{m}\frac{v_x}{v_y} + \frac{C_\varphi}{m}\varphi + \frac{C_\delta}{m}\delta \tag{2}$$

$$\dot{p} = \frac{1}{I_x}(E_r r + E_p p + E_\beta \frac{v_x}{v_y} + E_\varphi \varphi + E_\delta \delta) \tag{3}$$

$$\dot{r} = \frac{1}{I_Z}(D_r r + D_p p + D_\beta \frac{v_x}{v_y} + D_\varphi \varphi + D_\delta \delta) \tag{4}$$

where

$$C_r = \frac{\partial F_y}{\partial r} = -\frac{a_1}{v_x} C_{af} + \frac{a_2}{v_x} C_{ar} \tag{5}$$

$$C_p = \frac{\partial F_y}{\partial p} = \frac{C_{af}C_{\beta f}}{v_x} + \frac{C_{ar}C_{\beta r}}{v_x} \tag{6}$$

$$C_\beta = \frac{\partial F_y}{\partial \beta} = -(C_{af} + C_{ar}) \tag{7}$$

$$C_\varphi = \frac{\partial F_y}{\partial \varphi} = C_{ar}C_{\delta\varphi r} + C_{af}C_{\delta\varphi f} - C_{\varphi f} - C_{\varphi r} \tag{8}$$

$$C_\delta = \frac{\partial F_y}{\partial \delta} = C_{af} \tag{9}$$

$$D_r = \frac{\partial M_z}{\partial r} = -\frac{a_1^2}{v_x}C_{af} - \frac{a_2^2}{v_x}C_{ar} \tag{10}$$

$$D_p = \frac{\partial M_z}{\partial p} = \frac{a_1}{v_x}C_{\beta f}C_{af} - \frac{a_2}{v_x}C_{\beta r}C_{ar} \tag{11}$$

$$D_\beta = \frac{\partial M_z}{\partial \beta} = -(a_1C_{af} - a_2C_{ar}) \tag{12}$$

$$D_\varphi = \frac{\partial M_z}{\partial \varphi} = -a_1\left(C_{\varphi f} - C_{af}C_{\delta\varphi f}\right) + a_2\left(C_{\varphi r} - C_{ar}C_{\delta\varphi r}\right) \tag{13}$$

$$D_\delta = \frac{\partial M_z}{\partial \delta} = a_1C_{af} \tag{14}$$

$$E_r = \frac{\partial M_z}{\partial r} = -\frac{a_1}{v_z}C_{Tf}C_{af} + \frac{a_2}{v_z}C_{Tr}C_{ar} \tag{15}$$

$$E_p = \frac{\partial M_z}{\partial p} = \frac{1}{v_z}C_{\beta f}C_{Tf}C_{af} + \frac{1}{v_z}C_{\beta r}C_{Tr}C_{ar} - c_\varphi \tag{16}$$

$$E_\beta = \frac{\partial M_z}{\partial \beta} = -C_{Tf}C_{af} - C_{Tr}C_{ar} \tag{17}$$

$$E_\varphi = \frac{\partial M_z}{\partial \varphi} = -C_{Tf}\left(C_{\varphi f} - C_{af}C_{\delta\varphi f}\right) - k_\varphi - C_{Tr}\left(C_{\varphi r} - C_{ar}C_{\delta\varphi r}\right) \tag{18}$$

$$E_\delta = \frac{\partial M_z}{\partial \delta} = C_{Tf}C_{af} \tag{19}$$

In the above equations, the steer angle δ acts as the input, and there is a total of four differential equations of motion. In this paper, assume v_x to be a varying parameter for a third-order system constructed by Equations 2-4. The tire forces are assumed to be proportional to the side-slip angles; also, the right and left tires' cornering stiffnesses are assumed to be similar and equal to half of the entire axle's.

STEADY-STATE RESPONSES

By using the bicycle-roll vehicle model, the primary vehicle responses at steady-state turning are defined for the steer angle input for a front-wheel steering vehicle. At steady-state turning, the time derivative of the variables are equal to zero, and the equations of motion can be simplified to a set of algebraic equations. The steady-state curvature, yaw rate, and side-slip responses which are used in this study are derived and simplified as:

$$S_\kappa = \frac{k}{\delta} = \frac{1}{\rho\delta} = -\frac{Z_1}{v_x Z_0} \tag{20}$$

$$S_r = \frac{r}{\delta} = \frac{k}{\delta} v_x = S_k v_x = -\frac{Z_1}{Z_0} \tag{21}$$

$$S_\beta = \frac{\beta}{\delta} = \frac{Z_2}{Z_0} \tag{22}$$

where Z_0, Z_1, Z_2 are given as:

$$Z_0 = E_\beta\left(D_r C_\varphi - C_r D_\varphi + m v_x D_\varphi\right) + E_\varphi\left(C_r D_\beta - D_r C_\beta - m v_x D_\beta\right) + E_r(C_\beta D_\varphi - D_\beta C_\varphi) \tag{23}$$

$$Z_1 = E_\beta\left(C_\varphi D_\delta - v_x C_\delta D_\varphi\right) - E_\varphi\left(C_\beta D_\delta - v_x C_\delta D_\beta\right) + E_r\left(C_\beta D_\varphi - D_\beta C_\varphi\right) \tag{24}$$

$$Z_2 = E_\phi(D_\delta m v_x + C_\delta D_r - C_r D_\delta) + \left(C_\phi D_\delta - C_\delta D_\phi\right)E_r + \left(C_r D_\phi - C_\phi D_r - D_\phi m v_x\right)E_\delta \tag{25}$$

3) VEHICLE BEHAVIOUR

Ground vehicles work in steady-state conditions most of the time. The planar vehicle motion at any instant may be described by being in steady-state or transitioning between two steady-state conditions. The steady-state response of vehicles is dominant in typical public street driving conditions when the velocity and steer angle inputs are constant or changing slowly. The transient effect of passenger vehicles is almost negligible in terms of the response of dynamic variables'. This feature of the vehicle dynamics allows us to plot a steady-state chart for the local coordinates of the instantaneous centre of rotation (ICR) of the bicycle-roll vehicle model in the body-fixed frame (Figure 2). Figure 2 shows that the lateral position of the ICR mainly depends on the steer angle input from the driver and the longitudinal position is mainly affected by the forward velocity.

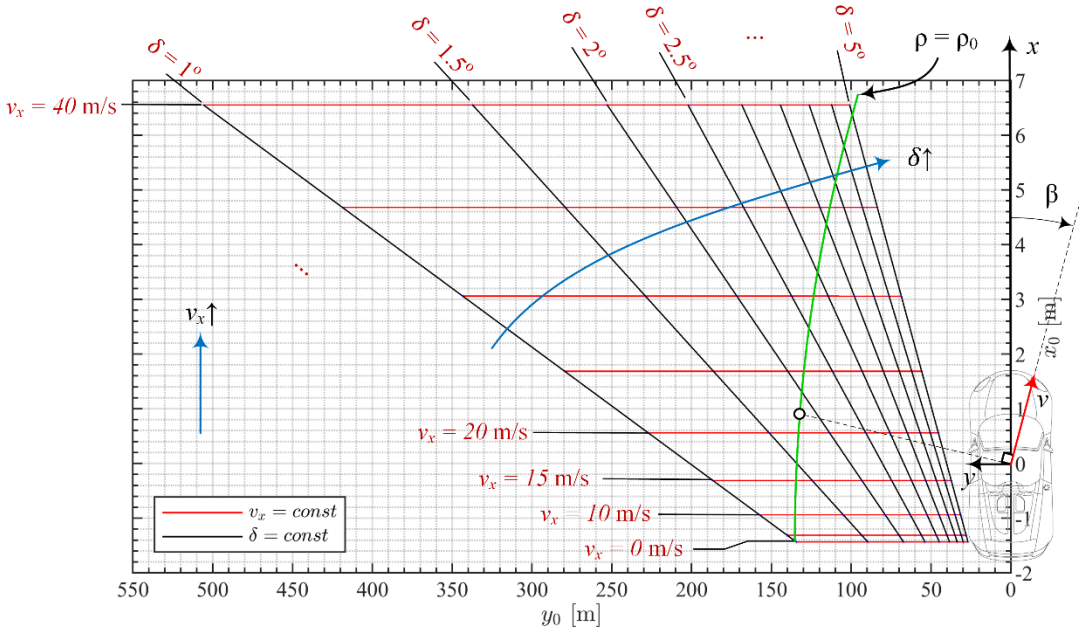

Figure 2: ICR Coordinate in Body Frame (not in scale)

Note that the constant steer angle and constant velocity curves in Figure 2 are not exactly linear. For a given radius of rotation ρ_0, the side-slip angle β is dictated by the selection of v_x or δ. Theoretically, let δ be free and assume there is no friction limit under the tires, the vehicle may negotiate a given turn with any velocity at the expense of going under some induced side-slip angle which is not necessarily desirable. To negotiate a turn with a given radius, the ICR must be at the same distance from the vehicle body frame; by choosing the desired velocity, the required steer angle is determined. The sample point P illustrated in the figure shows that for the velocity of 20 m/s, it requires a steering angle of around 1.75 degrees to stay on a circular road with radius ρ_0. Considering velocity as the given limiting factor, using Equations 17 and 19, the required steer angle to keep a radius of turning ρ is obtained as a function of velocity as:

$$\delta_\rho = \delta_\rho(v_x) = -\frac{v_x Z_0}{\rho Z_1} \tag{26}$$

$$\beta_\rho = \beta_\rho(v_x) = \frac{\delta_\rho Z_2}{Z_0} = -\frac{v_x Z_2}{\rho Z_1} \tag{27}$$

which is visualised in Figure 3 for the vehicle of interest. The values of vehicle parameters are as follows:

$C_{\alpha f} = 52000$ N/rad $\quad C_{\alpha r} = 72000$ N/rad $\quad m = 845.4$ kg $\quad I_z = 1490$ kgm^2 $\quad I_x = 350$ kgm^2

$a_1 = 0.909$ m $\quad a_2 = 1.436$ m $\quad k_\varphi = 26612$ Nm/rad $\quad c_\varphi = 1700$ Nms/rad

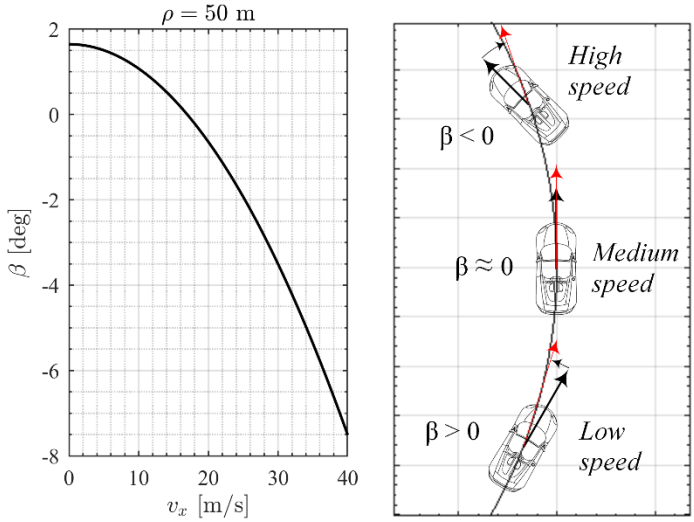

Figure 3: Variation of side-slip angle versus velocity for a constant radius of curvature

4) AUTONOMOUS CONTROL

IMPROVED AUTODRIVER ALGORITHM

Vehicles in motion on the road are always turning about the curvature centre of the road at the right curvature radius. If we consider a given road $\mathbf{r} = \mathbf{r}\ (X, Y, Z, \psi)$ to be a three-dimensional spatial curve, and the vehicle to be driven in the osculating plane, we can calculate the path of curvature centre in the osculation plane, both in the global coordinate and the vehicle body coordinate frames. The desired location of the road curvature centre must coincide with the vehicle's rotation centre. If correct inputs δ, v_x are selected, there is no error between the actual position of the vehicle, ${}^{G}\mathbf{r} = {}^{G}\mathbf{r}\ (X, Y, Z, \psi)$ with the desired position ${}^{G}\mathbf{r}_d = {}^{G}\mathbf{r}_d\ (X, Y, Z, \psi)$. The loci of curvature centre for two sample roads are shown in Figure 4.

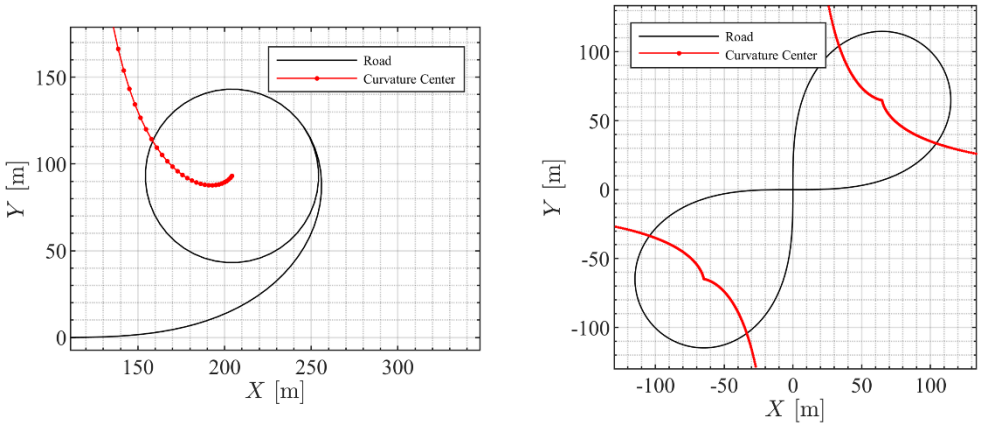

Figure 4: Sample Roads and their Curvature Centres

Based on the discussion in section II, ideally, we are able to keep the vehicle on any curve as long as we choose the correct steer angle and velocity from the ICR chart (Figure 2) to coincide the ICR with the curvature centre of the road in the vehicle body coordinate frame. Although this solution is correct as the final value, due to the transient period dynamics, it cannot completely eliminate the error between the path of motion and the road. In other words, the overall path of motion would have a similar shape to the road curve, but there would be an increasing offset as the vehicle moves forwards due to an initial error during

the transient stage. To compensate the transient error of path-following, a feedback controller is designed in the following section.

Calculation of Steady-State Inputs

It can be seen from the axes scales that the steering angle mainly determines the turning radius of the vehicle. Although the velocity does make some contribution to the ICR location, its effect is minor, especially for small side-slip angles. Therefore, we should assume that the main contribution on the radius of rotation is coming from the steer angle and $y_0 \approx \rho_0$. Thus, the steering angle should be set to position the ICR laterally correctly (regulating y_0); then the vehicle running at a given velocity will eventually gain the side-slip angle β dictated by the velocity, which causes the longitudinal position of ICR in the body coordinate to match the road curvature centre. The desired velocity is usually given as a velocity profile for different sections of the road.

Elimination of Transient Error

In addition to the ICR, the actual global position of the vehicle is calculated as

$$X = \int_0^t v_x \cos\psi - v_y \sin\psi \; dt \tag{28}$$

$$Y = \int_0^t v_x \sin\psi + v_y \cos\psi \; dt \tag{29}$$

which are solved together with Equations 2-4 on the basis of the approximated inputs coming from steady-state analysis. Any lateral position error in the vehicle's body frame may be compensated by adjusting the steering angle, and any longitudinal position error in the vehicle's body frame may be compensated by adjusting the vehicle's forward acceleration, and hence the velocity. Road constraint implies that there would be no error in the Z direction. The overall algorithm may be summarised in the following steps:

1. A desired path of motion is given in 3D as ${}^G\mathbf{r}_d = {}^G\mathbf{r}_d\left(X_d(s), Y_d(s), Z_d(s)\right)$ as a function of arc length s,
2. Differential geometry provides us with location of the road curvature centre in global coordinates ${}^G\mathbf{r}_c = {}^G\mathbf{r}_c\left(X_c(s), Y_c(s), Z_c(s)\right)$,
3. Kinematic transformation provides the coordinates of interest (road and its curvature centre) in the vehicle body coordinate frame as: ${}^B\mathbf{r}_d = [x_d \;\; y_d \;\; z_d]^T = {}^BR_G \, {}^G\mathbf{r}_d$, ${}^B\mathbf{r}_c = [x_c \;\; y_c \;\; z_c]^T = {}^BR_G \, {}^G\mathbf{r}_c$,
4. Steady-state equations determine the required steer angle $\delta_{ss}(s)$ for a given speed v_x and a radius of rotation ρ in order to laterally coincide the rotation centre of the vehicle with curvature centre of the road.
5. The lateral error between the desired vehicle position and its actual position in body coordinate frame $e_y = y_d - y = y_d$ is fed into a feedback controller. The controller provides $\delta_e(s)$ to adjust the total steer angle $\delta = \delta_{ss} + \delta_e$ to eliminate the lateral position error.
6. The longitudinal error between the desired vehicle position and its actual position in the body coordinate frame $e_x = x_d - x = x_d$ is fed into a longitudinal feedback controller which provides $\dot{v}_x$ to adjust forward velocity and eliminate the longitudinal position error.

As mentioned in steps 1 & 2 above, the desired vehicle location (the road) is a function of the distance travelled. However, we may alternatively assume them to be functions of time:

$${}^G\mathbf{r}_d = {}^G\mathbf{r}_d\left(X_d(t), Y_d(t), Z_d(t)\right), \quad {}^G\mathbf{r}_c = {}^G\mathbf{r}_c\left(X_c(t), Y_c(t), Z_c(t)\right)$$

This assumption defines the ideal vehicle as the one running at a constant given velocity v_{x0} on the road, without any offset. In other words, the ideal vehicle is considered a kinematic model which can negotiate any turn regardless of the velocity and the road curvature. Thus, the effect of dynamic turning is not included for the ideal vehicle motion. Such a concept for a moving vehicle is called a Ghost-Car approach. In this paper, we set the Autodriver algorithm's target to follow the ideal Ghost-Car on the road and minimise the offset at any time. Figure 5-a visualises the Ghost-Car and the error definitions, all expressed in the vehicle's body coordinate frame.

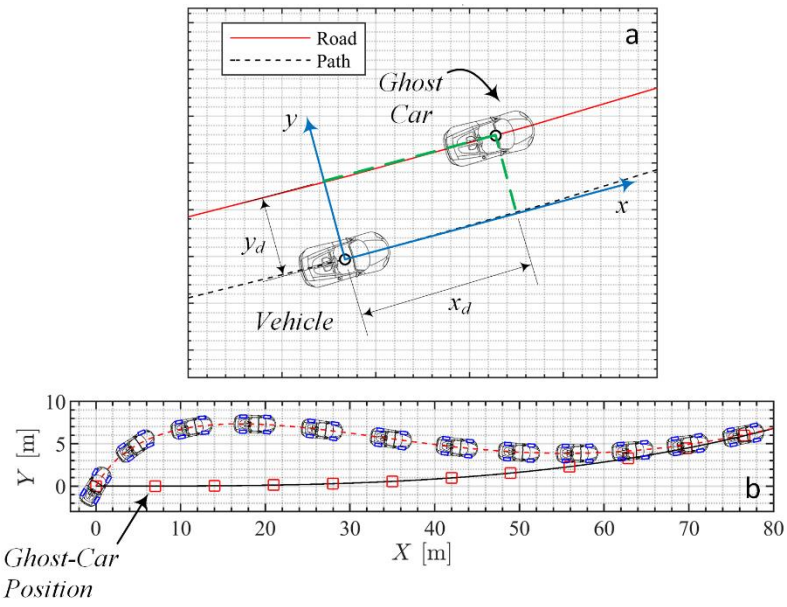

Figure 5a: A visualises the Ghost-Car Error values expressed in body frame

Figure 6b: path-following strategy using the Ghost-Car approach

An example of a path-following strategy using the Ghost-Car approach is shown in Figure 5-b.

CONTROL

In terms of control terminology, the control layout consists of a feedforward part working on the basis of steady-state vehicle behaviour, and two feedback loops to compensate for transient errors and keeping the vehicle on the desired point of the road at any time instance. Figure 7 shows the proposed control structure.

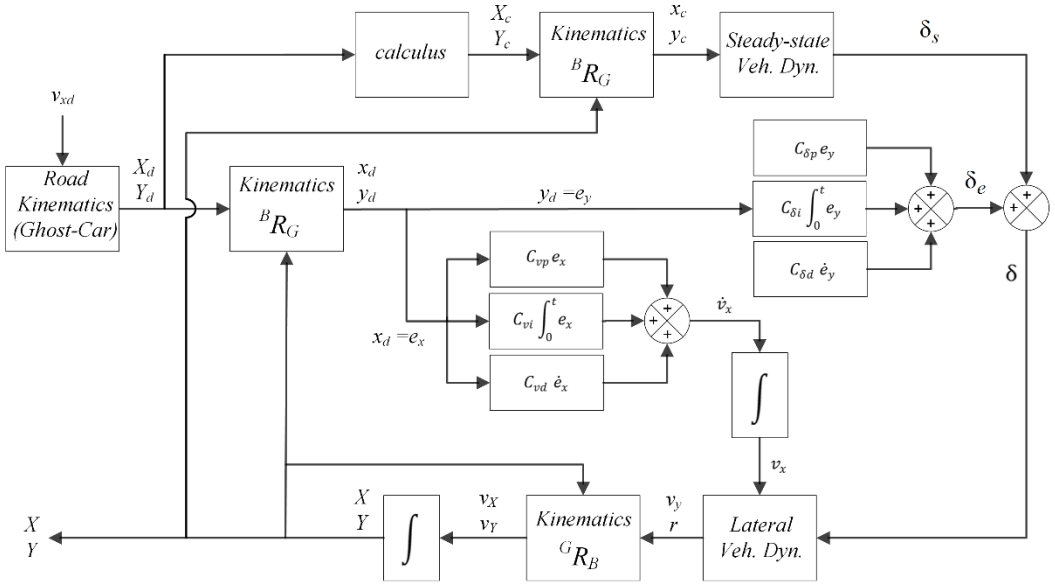

Figure 7: Block diagram of the control system structure

The feedforward provides a quick response of the control system based on the available road data. The steady-state behaviour may estimate the vehicle response with considerably good accuracy. Thus, the steady-state behaviour is chosen for the feedforward part of the lateral controller. The inclusion of feedforward assures that the central portion of the control input is provided to the vehicle as soon as it reaches a turn. The transient error, however, needs to be fully compensated in order to achieve a reliable autonomous path-following performance. Due to the high level of accuracy of the feedforward, a simple PD feedback control is sufficient to close the control loop. Two errors are to be minimised, namely the longitudinal and the lateral position errors expressed in the vehicle body coordinate frame e_x, e_y. The lateral position error is compensated with a correction signal added to the previously calculated steer angle.

Minimisation of the longitudinal position error requires manipulation of the vehicle's longitudinal velocity. Since a sudden change in velocity cannot happen in a real vehicle, we take its time derivative $\dot{v}_x$ as the control variable for longitudinal adjustment which corresponds to a precise acceleration command to the engine or brakes. The total longitudinal acceleration is given as $a_x = \dot{v}_x - r v_y$, but we only have direct control over $\dot{v}_x$ by the throttle/brake command.

As we have a position control problem, the regulated outputs are, in fact, results of the integration of the vehicle's dynamic variables v_x, v_y and r. Therefore, a PD controller would be desirable with the equal part having a similar effect to an integrator controller on a first-order system, and the derivative part acts as a proportional controller. This would be equivalent to the effect of a PI controller on the system. Thus, the PD controller is expected to minimise the steady-state error while the feedforward part provides a quick response. The PD gains are tuned manually in this paper. For longitudinal control $C_{vp} = 1,\ C_{vd} = 1$ and for lateral control $C_{\delta p} = 0.01,\ C_{\delta d} = 0.025$.

5) SIMULATION RESULTS

To investigate the effectiveness of the proposed path-following controller, two scenarios were simulated with different road geometries. It is worth noting that an ideal transition between two sections of a road with constant curvatures is achieved using a linearly changing curvature function, rather than connecting the two sections by making them tangent to each other. Such a linearly changing curvature (e.g. clothoid) provides a linearly changing steer angle requirement with no jump, which is physically feasible. The clothoid is defined using Fresnel integrals as follows (Marzbani, Jazar & Fard 2015):

$$X = a\int_0^t \cos(\frac{\pi}{2}u^2)\,du = a\int_0^{s/a} \cos(\frac{\pi}{2}u^2)\,du \tag{30}$$

$$Y = a\int_0^t \sin(\frac{\pi}{2}u^2)\,du = a\int_0^{s/a} \sin(\frac{\pi}{2}u^2)\,du \tag{31}$$

where parameter a is the scaling parameter and determines the size of the clothoid and t is the independent variable which may be converted to arc length $s = at$ for simplicity. By using clothoid in road geometry construction, a smoother performance of the driver's steering control is expected in the case of a linear curvature change.

Figure-of-8 Road

The first scenario investigates the controller's performance on a road which is designed on the basis of transitions between zero and constant curvature ($\kappa = 1/\rho = 0.02$) sections forming an 8-shaped geometry. Such a road geometry is a desirable example to evaluate the controller on. It includes straight parts at the origin while having constant curvature turns (circular arcs) at both ends. The transition between left and right turns as well as driving into turns are examined at the same time using this road geometry. The transitions are achieved using clothoids keeping the curvature of the road continuous throughout the entire road. The clothoids are constructed based on a scaling of $a = 147.195$ and a total arc length of $s_1 = 137.9$ m.

Figure 8 shows the road geometry and the vehicle's path of motion starting from the origin towards the positive x-axis. The initial and desired velocity of the vehicle is set at 20 m/s. The path of motion shows a high accuracy of path following achieved by the Autodriver algorithm.

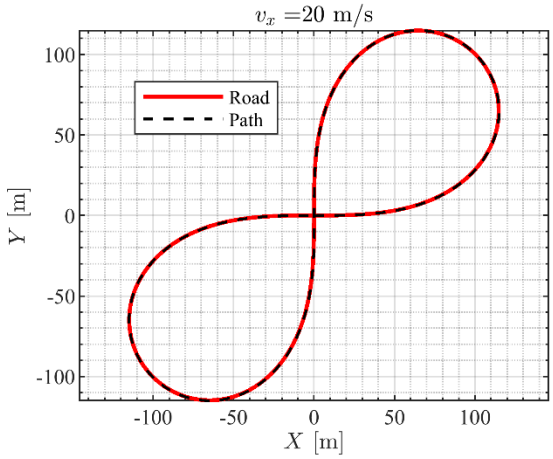

Figure 8: Figure-of-8 road and vehicle's path of motion

The required steer angle and the instantaneous velocity of the vehicle are shown in Figure 9. It is observed that the steer angle is continuous with negligible fluctuations in order to overcome the transient error. The velocity of the vehicle is also kept very close to the desired value (20 m/s) with very small variations to compensate for the longitudinal error with respect to the Ghost-Car.

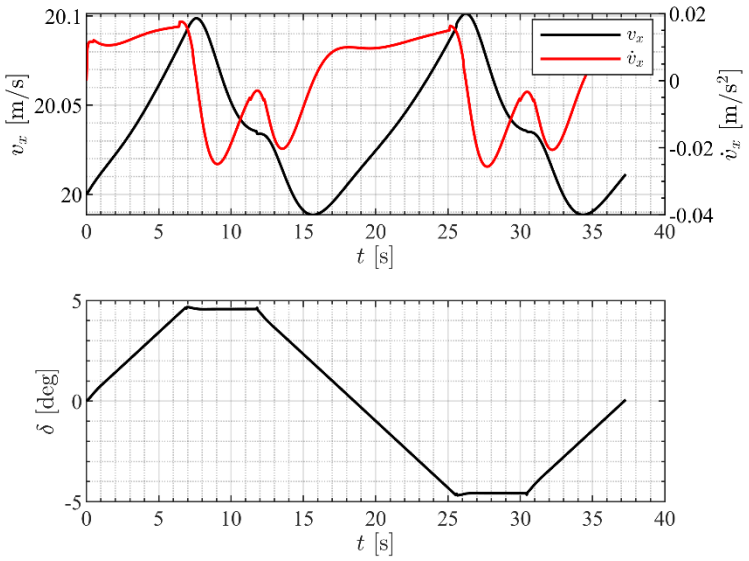

Figure 9: Provided velocity and steer angle for figure-8 Road

Figure 10 shows the time history of the dynamic variables of the system. The continuous and proportional increase in the variables shows a smooth control performance. The negative side-slip angle β and large roll angle of $\phi = 5\ deg$ show a relatively high velocity condition (Figure 3) and sharpness of the turn corresponding to the vehicle running at 20 m/s. The small roll rate p history also proves the smooth performance of the controller which provides more comfort to the passengers during such a tight turn. The yaw velocity r is also consistent with the road geometry and does not show fluctuations, thus maximising the passenger comfort.

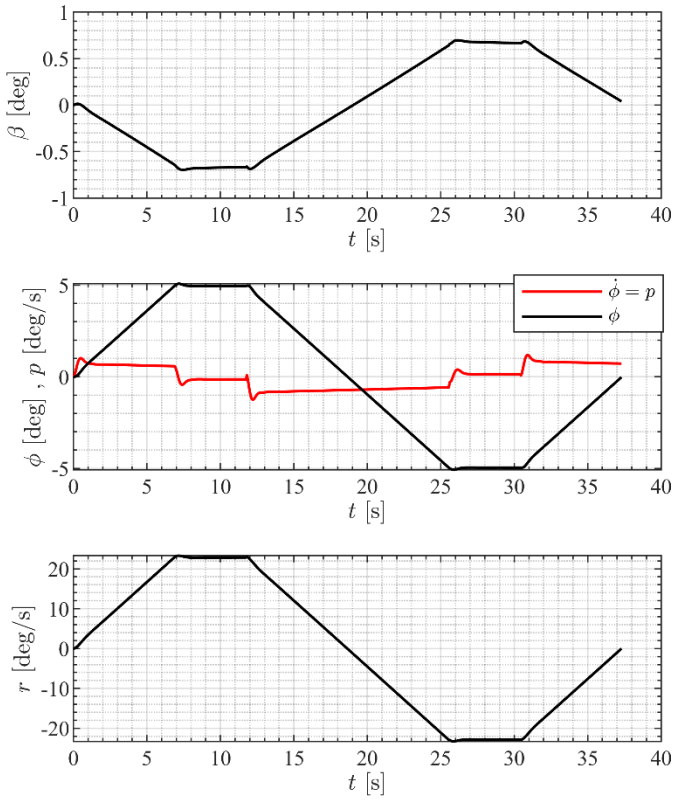

Figure 10: Vehicle's dynamic variables for figure-8 road

The longitudinal and lateral error values in the body frame are depicted in Figure 11-a,b. The longitudinal error is negligible, which is handled by the velocity controller. It shows that the vehicle successfully followed the Ghost-Car on the road with minor errors. The lateral error Δy gets a maximum of 0.2 m during the maneuver which is considered a very good path-following performance at a velocity of 20 m/s and a sharp turn with a radius of 50 m. Assuming a lane width of 3 – 3.5 m, the common passenger vehicles have approximately 0.5 – 0.75 m from each side to reach the lane margin which is well above the achieved error range.

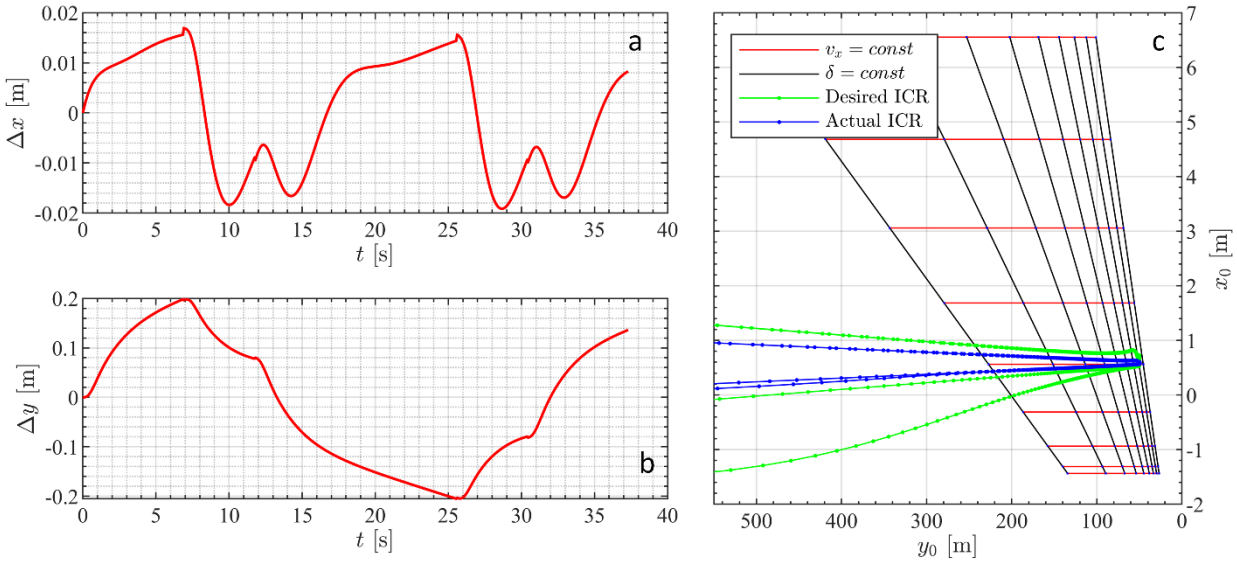

Figure 11a: Following Errors in Body Frame for Figure-8 Road in x-direction.

Figure 12b: Following Errors in Body Frame for Figure-8 Road in y-direction.

Figure 13c: The location of ICR in the body frame attached to the vehicle

The location of ICR in the body frame attached to the vehicle is shown in Figure 11-c. The green loci show the desired points for ICR and the blue loci indicate the actual locations of ICR during the manoeuvre. It is observed that both curves converge to the same location in steady-state with minor deviation.

LANE CHANGE MANOEUVRE

Another important manoeuvre for evaluation of the path-following control is the lane-change manoeuvre. Such a manoeuvre is very popular in the literature and also a quite common practice in every-day driving as well as obstacle-avoidance scenarios. To model the desired path rationally, we perform four different scenarios with the lane-change virtual road created using clothoids, and with a final section made of a straight line (Figure 14). The clothoids are constructed based on a scale of $a = 80$ and a total arc length of $s_1 = 15$ m. The Autodriver algorithm successfully drove the vehicle on the intended path at a longitudinal velocity of 20 m/s causing the vehicle to displace 3.5 m laterally within 60 m of distance travelled.

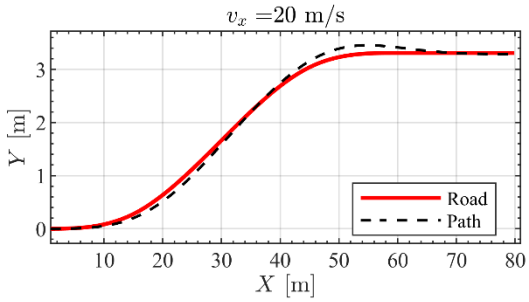

Figure 14: Lane-Change Virtual Road and Vehicle Path

Figure 15 shows the velocity adjustment by the controller to follow the Ghost-Car as well as the required steer angle. Due to the short distance travelled and small curvature of the path, the required adjustment in longitudinal acceleration of the vehicle is negligible which is a desirable condition from comfort perspective. The steer angle history shows continuous behaviour proving the smooth operation of the system. It is

important to note that the proportional behaviour of the steer angle is imposed by the selected road geometry with linearly changing curvature and it does not represent the only way of performing a lane-change.

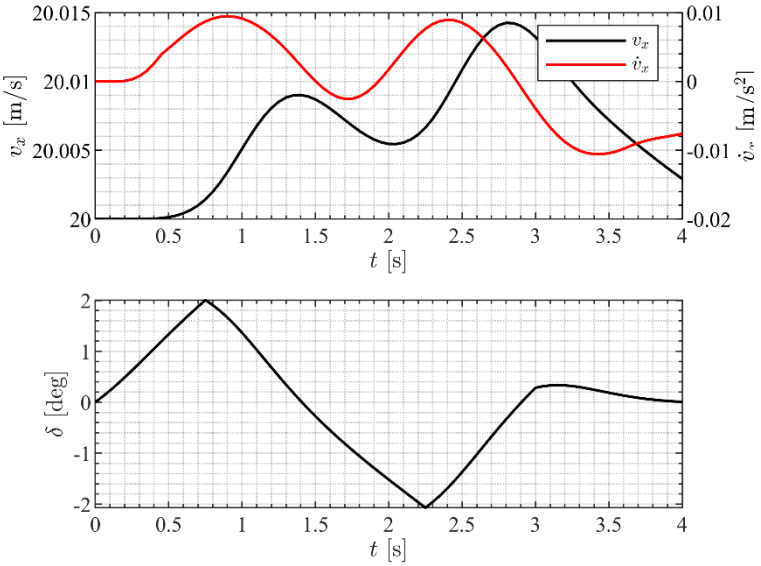

Figure 15: Provided Velocity and Steer Angle for Lane-Change Maneuver

Vehicle response is depicted in Figure 16 in terms of its dynamic variables. Negative side-slip angle appeared because of the relatively high vehicle velocity while the maximum roll angle was relatively small due to the small curvature of the path. The roll rate p, however, is larger than the previous manoeuvre because of the sudden nature of the lane-change manoeuvre. In other words, the vehicle is steered back and forth before it settles at a steady-state. Yaw velocity behaviour of the vehicle is smooth proving a desirable performance in terms of passenger comfort.

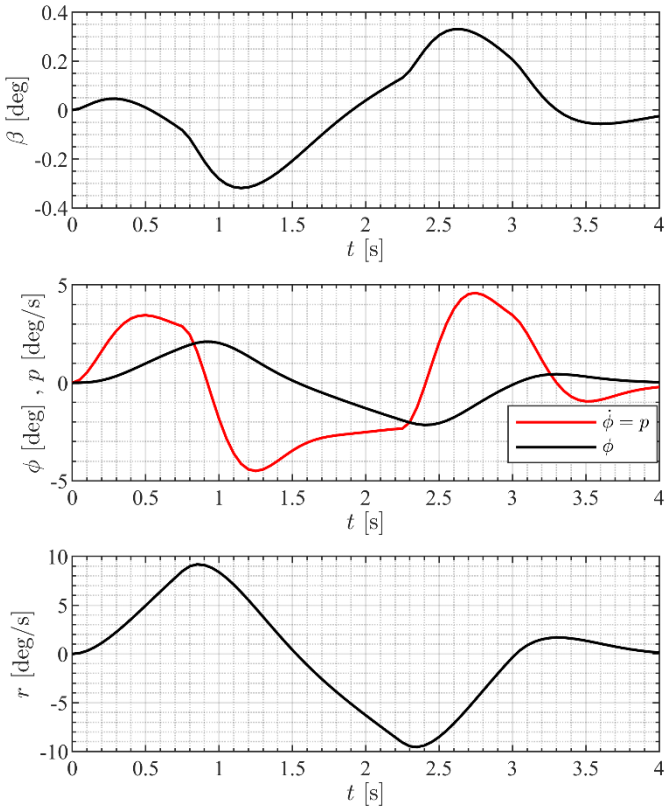

Figure 16: Vehicle's Dynamic Variables for Lane-Change Maneuver

Longitudinal and lateral errors between the actual and desired vehicle location throughout the manoeuvre are shown in Figure 17-a,b. The longitudinal error is negligible due to the small curvature and short travel distance, proving the excellent Ghost-Car following ability of the system. The lateral error is also negligible at such a relatively high-speed. The maximum lateral error is less than 0.2 m in the returning cycle (second half of the lane-change action, between approximately 0 and 30 m travelled). This is due to the nonzero initial yaw and lateral velocities in the return cycle (from 30 m to 60 m). In other words, the second stage of lane-change will result in an overshoot in the lateral following error.

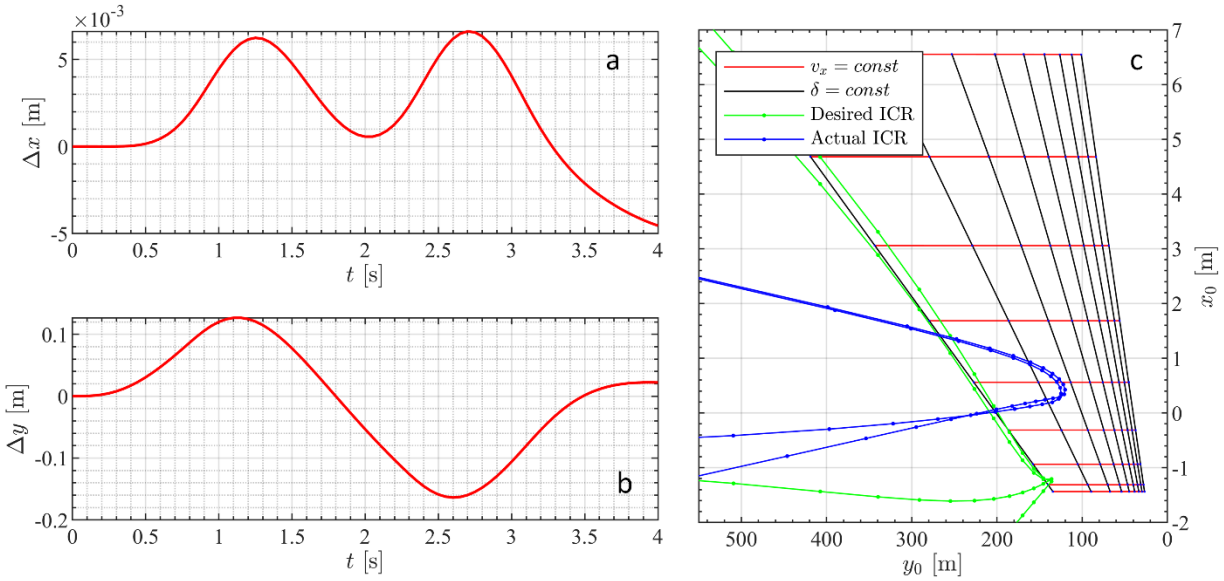

Figure 17a: Following errors in body frame for lane-change maneuver in x-direction.

Figure 18b: Following errors in body frame for lane-change maneuver in y-direction.

Figure 19c: The ICR loci in the body coordinate

The ICR loci in the body coordinate is plotted and shown in Figure 17-c. The transient nature of the manoeuvre is also observed in this figure. The ICR does not reach the desired (steady-state) location during the lane change, but the difference is small, proving the effectiveness of using a steady-state response as feed-forward and overall control performance, even for sudden manoeuvres.

6) CONCLUSIONS

In conclude, in order to cope with the practical implementations, an autodriver algorithm was improved to adjust the vehicle position on the desired road with a feed-forward-feedback control algorithm. The steady-state lateral response was used to accelerate the controller performance in terms of steering, while the transient error was eliminated with feedback control. Meanwhile, the longitudinal error was determined using a Ghost-Car concept to follow the road at the desired speed by manipulating the longitudinal acceleration of the vehicle via feedback control.

It is worth mentioning that any small error between the locations of the vehicle and the road will be amplified in the location error of ICR; therefore, by starting from ICR placement and then adjusting transient position errors, an accurate and quick performance was achieved which is critical for autonomous vehicle control. Simulations are performed for the figure-of-8 and lane-change manoeuvres, which are comprehensive indicators of different driving conditions. The results show promising performance of the algorithm in terms of path-following, even under sudden manoeuvring requirements. The algorithm was evaluated using a more realistic vehicle model (roll model), including the roll motion. Observation of roll behaviour also proved the desirable performance of the controller in terms of passenger comfort, proving the efficiency of the proposed algorithm both for path-following and passenger comfort. Ideally, to minimise the roll rate, a vehicle can control the roll so that occupants can enjoy the comfort inside the vehicle, which fulfils the objective of the research.

REFERENCES

[1] Bishop, R 2005, Intelligent vehicle technology and trend, Artech House, Norwood, MA.

[2] Gajek A.: Directions for the development of periodic technical inspection for motor vehicles safety systems. *The Archives of Automotive Engineering – Archiwum Motoryzacji.* 2018;80(2):37-51. DOI:10.14669/AM.VOL80.ART3.

[3] Hansson L.: Regulatory governance in emerging technologies: The case of autonomous vehicles in Sweden and Norway, *Research in Transportation Economics, 2020, 83, 100967*, DOI:10.1016/j.retrec.2020.100967.

[4] Hasan M. H., Hentenryck P.: The benefits of autonomous vehicles for community-based trip sharing, Transportation Research Part C: *Emerging Technologies, 2021, 124, 102929*, DOI:10.1016/j.trc.2020.102929.

[5] Hong Z. L., Zimmerman N.: Air quality and greenhouse gas implications of autonomous vehicles in Vancouver, Canada, Transportation Research Part D: Transport and Environment, 2021, 90, 102676, DOI:10.1016/j.trd.2020.102676

[6] Masmoudi M., Ghazzai H., Frikha M., et al.: Object Detection Learning Techniques for Autonomous Vehicle Applications, 2019 IEEE International Conference on Vehicular Electronics and Safety (ICVES), Cairo, Egypt, 2019, 1-5, DOI: 10.1109/ICVES.2019.8906437

[7] Molina C. B. S. T., Almeida J. R. d., L. F. Vismari, et al.: Assuring Fully Autonomous Vehicles Safety by Design The Autonomous Vehicle Control (AVC) Module Strategy, *2017 47th Annual IEEE/IFIP International Conference on Dependable Systems and Networks Workshops (DSN-W), Denver, CO, 2017, 16-21*, DOI: 10.1109/DSN-W.2017.14.

[8] Mrowicki A., Kubiak P., Zakrzewicz W.: Nonlinear method of precrash velocity determination for Mini car class-B-spline tensors products with probabilistic weights. *The Archives of Automotive Engineering – Archiwum Motoryzacji*. 2020;87(1):97-108. DOI:10.14669/AM.VOL87.ART8.

[9] Qingwen Xue, Ke Wang, Jian John Lu, Yujie Liu : Rapid Driving Style Recognition in Car-Following Using Machine Learning and Vehicle Trajectory Data. *Journal of Advanced Transportation 2019*. DOI:10.1155/2019/9085238

[10]Santana E. F. Z., Covas G., et al.: Transitioning to a driverless city: Evaluating a hybrid system for autonomous and non-autonomous vehicles, Simulation Modelling Practice and Theory, 2021, 107, 102210, DOI:10.1016/j.simpat.2020.102210.

[10] Seyfettin Vadi, P. Sanjeevikumar, F. Blaabjerg, R. Bayindir. 2019 A Review on Optimization and Control Methods Used to Provide Transient Stability in Microgrids, doi: 10.3390/en12183582

[11] Sung K., Min K., Choi J.: Driving information logger with in-vehicle communication for autonomous vehicle research, 2018 20th International Conference on Advanced Communication Technology (ICACT), Chuncheon-si Gangwon-do, Korea (South), 2018, 300-302, doi: 10.23919/ICACT.2018.8323732.

[12] Todorovic M., Simic M., Kumar A.: Managing Transition to Electrical and Autonomous Vehicles, Procedia Computer Science, 2017, 112, 2017, 2335-2344, DOI:10.1016/j.procs.2017.08.201.

[13] Wang J. et al.: Appearance-based Brake-Lights recognition using deep learning and vehicle detection, 2016 IEEE Intelligent Vehicles Symposium (IV), Gothenburg, Sweden, 2016, 815-820, doi: 10.1109/IVS.2016.7535481.